

## Plastic Deformation of Single Nanometer-Sized Crystals

Litao Sun,<sup>1,2</sup> Arkady V. Krasheninnikov,<sup>3,4</sup> Tommy Ahlgren,<sup>3</sup> Kai Nordlund,<sup>3</sup> and Florian Banhart<sup>5,\*</sup>

<sup>1</sup>Key Laboratory of MEMS of Ministry of Education, Southeast University, Nanjing 210096, China

<sup>2</sup>Institut für Physikalische Chemie, Universität Mainz, D-55099 Mainz, Germany

<sup>3</sup>Materials Physics Division, University of Helsinki, P.O. Box 43, FI-00014, Finland

<sup>4</sup>Laboratory of Physics, Helsinki University of Technology, P.O. Box 1100, FI-02015, Finland

<sup>5</sup>Institut de Physique et Chimie des Matériaux IPCMS-GSI, UMR 7504, 23 rue du Loess, 67034 Strasbourg, France

(Received 17 April 2008; published 7 October 2008)

We report *in situ* electron microscopy observations of the plastic deformation of individual nanometer-sized Au, Pt, W, and Mo crystals. Specifically designed graphitic cages that contract under electron irradiation are used as nanoscopic deformation cells. The correlation with atomistic simulations shows that the observed slow plastic deformation is due to dislocation activity. Our results also provide evidence that the vacancy concentration in a nanoscale system can be smaller than in the bulk material, an effect which has not been studied experimentally before.

DOI: [10.1103/PhysRevLett.101.156101](https://doi.org/10.1103/PhysRevLett.101.156101)

PACS numbers: 61.72.Cc, 62.25.-g, 62.50.-p, 68.37.Og

Materials consisting of crystallites with sizes of a few nanometers have shown outstanding mechanical properties [1,2], for example, exceptionally high strength or hardness. Although such materials are already in use in industrial applications, their response to deformation and the mechanisms of inevitable creep at high temperature are still far from being understood. This is in part due to the deformation behavior of such systems which is fundamentally different from that in their bulk counterparts [3,4]. Another reason is the lack of direct experimental information on defect dynamics in nanocrystalline materials. The field is dominated by atomistic simulations [5–8] which, although they have provided much insight, are limited to the nanosecond time scale.

Several experimental attempts have been undertaken to study the deformation mechanisms in various systems of submicron dimensions. Information about the response of nanosystems to stress was obtained by measuring the electrical conductance of nanowires under straining [9]. *In situ* straining experiments on nanocrystalline bulk materials have been done in an electron microscope [10], and the role of grain-boundary-mediated processes versus dislocation activity was discussed. Experiments [11] on thin films and patterned lines also indicate that the early stage plasticity is strongly size-dependent. Thus, information on the plastic deformation of isolated nanometer-sized crystals may be crucial for understanding the deformation mechanisms in nanocrystalline materials, but it has not been studied experimentally to date.

Here we report experiments that allow the slow deformation of single nanocrystallites with simultaneous observation at the atomic scale by *in situ* high-resolution transmission electron microscopy (TEM). Metal crystals were exposed to pressure in graphitic nanocontainers that were designed for deformation experiments by electron beam structuring.

The principle of the experiment is shown schematically in Fig. 1. Graphitic nanocontainers are used as extrusion cells [12,13]. Au, Pt, Mo, and W crystals of a few nanometers in size were encapsulated inside graphitic shells by coevaporation in an arc discharge [14] and irradiated with electrons (300 keV) in a temperature range of 300–1000 °C in the heating stage of a TEM.

Under electron irradiation in a wide beam, the particles became spherical due to surface stress which is exerted by the graphitic shells upon the removal of atoms and reconstruction [15,16]. Then the electron beam was focused onto a spot of 2 nm in diameter and directed onto a point at the projected circumference of the graphitic shells. After 10–20 seconds, the puncturing caused a hole [13] (2–3 nm in diameter) through which the material under pressure could escape. Then the beam was spread again over the whole particle. During the continuing collapse of the shells [12,14,17], pressure was built up, and the solid metal was gradually extruded through the hole. Because of the slow contraction of graphitic shells, the deformation occurs on a

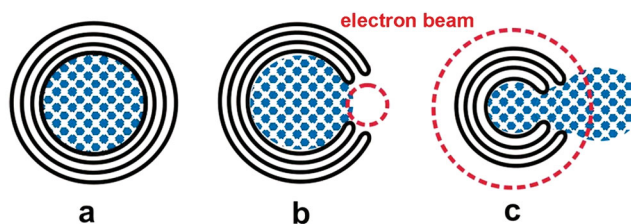


FIG. 1 (color). Mechanism of the experiment: Graphitic shells encapsulating a metal crystal (a) are punctured by a focused electron beam (b). Successive electron irradiation of the carbon container leads to the contraction of the shells and extrusion of the metal crystal (c). The red circles indicate the diameter of the electron beam.

scale of 0.1–1 nm/s. This allows us to study the stability of nanocrystals in detail under continuous load.

Figure 2 shows the gradual extrusion of a Au crystal from a graphitic shell ("carbon onion") at 300 °C. The puncturing of the shells was carried out between images (a) and (b). Grain boundaries appear repeatedly at the bottleneck in the Au crystal where the deformation rate is the highest. In other encapsulated Au crystals, twins were occasionally observed at 300 °C and below.

In the bulk regions of the crystals, both inside and outside, no visible defects appear. The faceting of the free Au surfaces outside the shells is apparent. The same experiment with Au at 600 °C is shown in Fig. 3. The process (a)–(f) happened within 12 minutes. No crystallographic defects appear, even in the bottleneck.

The same experiment with Pt (TEM images are shown in the supplementary material [18]) at 380 °C shows the formation of planar defects spreading over the whole crystal inside the shell. During the extrusion, stacking faults and twin boundaries appear, aligned in the direction of shear (through the hole). At 600 °C, the same behavior as for Au at 300 °C is seen (grain boundaries at the bottleneck, but no defects in the bulk). Further experiments were carried out with Pt up to 900 °C, showing qualitatively the same behavior as Au at 600 °C. The extrusion of Pt crystals is slower than for Au at the same temperature and under the same irradiation conditions.

The extrusion of Mo or W crystals (both in the fcc phase) turned out to be impossible within the temperature

range of these experiments (<1000 °C). The deformation of Mo or W crystals was much lower than of Au or Pt. It was always accompanied by the formation of grain boundaries or twins [14].

To obtain a quantitative value for the stress exerted onto the flowing crystals, we compared the lattice spacings in the crystals inside and outside the cell. This was done by Fourier transformation of the lattice images and measurement of the distances between the reflections [19]. These were relative measurements, always carried out from one micrograph. For example, in Fig. 2(b), the lattice spacing inside the container is 4% smaller than outside; in Fig. 3(d), we find a difference of almost 5%. Using the bulk modulus of gold (170 GPa), we obtain pressure differences of 15–25 GPa between inside and outside the shells. Hence, we can assume that a hydrostatic pressure of the order of 20 GPa prevails in the shell.

We can consider several deformation mechanisms to explain our observations: (1) material transport via self-

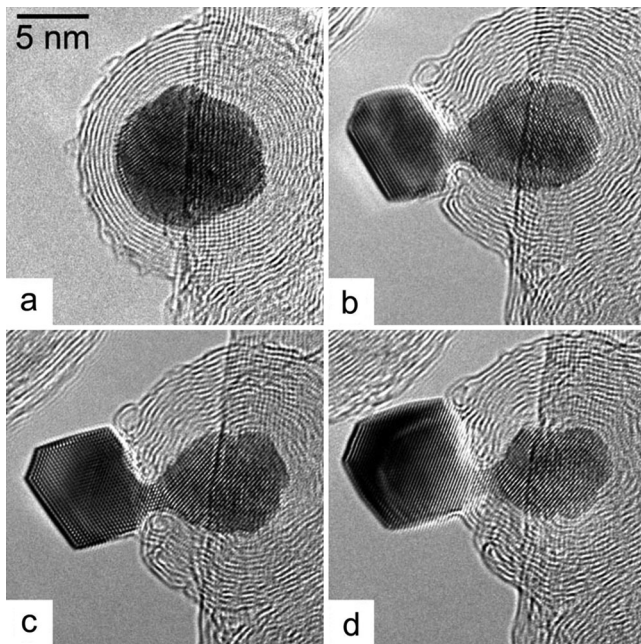


FIG. 2. Extrusion of a gold crystal from a punctured graphitic shell under electron irradiation at 300 °C. Grain boundaries appear at the bottleneck. Irradiation times: (a) 0, (b) 540, (c) 660, and (d) 900 s. Beam current density: 150 A/cm<sup>2</sup>. At 300 °C, the graphitic shells are defective due to slow annealing of radiation defects.

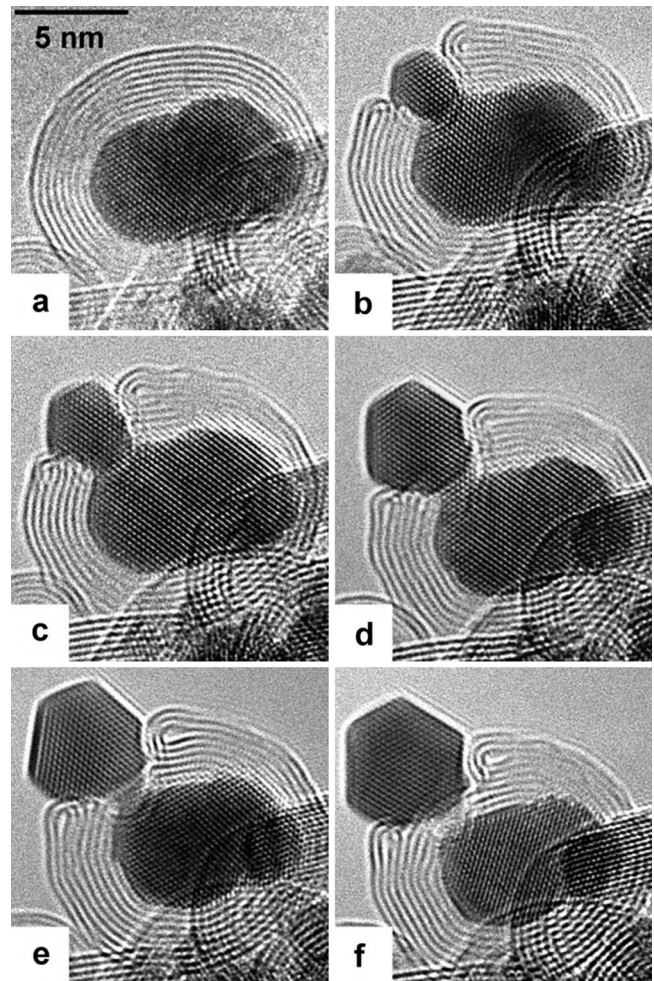


FIG. 3. Extrusion of a gold crystal at 600 °C. No visible defects appear in the Au crystal. Irradiation times: (a) 0, (b) 240, (c) 300, (d) 480, (e) 600, and (f) 720 s. Beam current density: 200 A/cm<sup>2</sup>. At 600 °C, the graphitic shells have a high structural perfection.

diffusion which can be associated with Herring-Nabarro creep; (2) diffusion of metal atoms at the metal-carbon interface (similar to Coble creep); and (3) plastic deformation due to the nucleation and glide of dislocations or the creation of planar defects.

High pressure in the nonextruded part of the metal particles indicates that the self-diffusivity (mechanism 1) or surface diffusivity (mechanism 2) must be slow; otherwise, no pressure buildup inside the opened shells would be possible. To check this conjecture, we calculated the material transfer due to self-diffusion at different temperatures and pressures; see [18] for details of calculations. We have assumed a vacancy concentration as in thermal equilibrium and that the vacancy formation energy  $E_f$  in the extruded part of the particle is the same as in the bulk system. We have taken the geometry of the experiment and assumed that diffusion is governed by vacancy migration. Hence, the vacancy flux is strongly influenced by a pressure gradient. Surprisingly, we found that the diffusion should be fast enough to provide efficient mass transfer for Au already at 300 °C and for Pt at 600 °C, which is inconsistent with the observation of considerable pressure (15–25 GPa) inside the cells.

An explanation of this pretended contradiction is that  $E_f$  in small crystals is higher than in the bulk, so that vacancy concentration and, correspondingly, self-diffusivity are low. This is a controversial issue: It has been previously suggested [20] that  $E_f$  should decrease with system size, as cohesive energy and melting temperature of a small particle drop. However, recent simulations [21] and our estimates [18] indicate that  $E_f$  can be larger for small particles than in the bulk systems. Our experimental results are consistent with a higher value of  $E_f$  for small particles and provide experimental evidence that the equilibrium vacancy concentration in small particles is indeed smaller than in bulk metals.

Similar arguments can be used to explain why mass transfer due to adatom diffusion (at the interface between metal and carbon) is suppressed. The separation between the graphitic shell and the metal in the uncompressed case is quite small (2–2.7 Å) [22]. Thus, it costs more energy (0.5–1 eV or more depending on pressure [18]) to place a metal atom into the space between the compressing graphitic shell and the metal than on a free metal surface, so it requires more than 3 eV to create an adatom-vacancy pair. Hence the carbon atom concentration at the metal-graphite interface should be negligible.

In order to explore the deformation by the nucleation and motion of dislocations, we carried out molecular dynamics computer simulations [18]. We concentrated on Pt as the typical fcc metal. The effect of contracting carbon shells on metal particles with typical diameters of about 4–8 nm (as in experiments) was modeled by an external repulsive potential mimicking the shrinking carbon shells.

Figures 4(a)–4(c) show the typical evolution of the system, and Fig. 4(d) presents the calculated internal pres-

sure  $P$  for a Pt particle with a diameter of 6 nm as a function of time or, correspondingly, the diameter of the repulsive external potential, as it changed linearly with time. The contraction of the shells gives rise to an increase in  $P$ , which is very slow in the beginning of the compression, as the systems can move as a whole and lower the energy by adjusting the positions of individual surface atoms. Then  $P$  increases almost linearly, which corresponds to the elastic regime. When  $P$  approaches the theoretical shear stress value, which for the potential we used is  $\sigma_T = 13.2$  GPa [18], a slip along a (111) plane happens, accompanied by a drop in the total energy of the system and a discontinuity in the pressure curve. The analysis of the evolution of the structure showed that the discontinuities are due to the formation of intrinsic stacking faults (ISFs) and twin boundaries. At high temperatures an ISF was normally formed by nucleation at the surface and very fast motion (at the time scale of 100 fsec) of a leading partial dislocation [23], leaving behind a planar

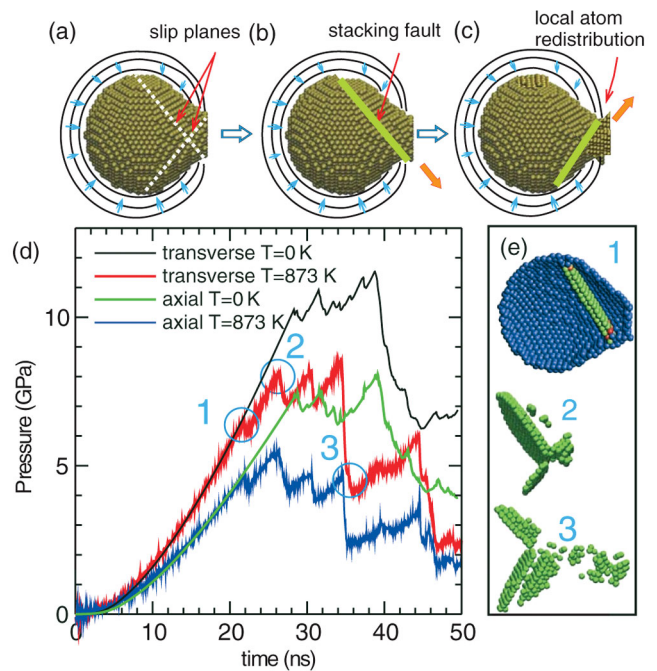


FIG. 4 (color). Molecular dynamics simulations of the extrusion of a platinum crystal from contracting graphitic shells. (a)–(e) Schematic illustration of the typical evolution of the system. (a) (111) slip planes are indicated by the dotted lines. Small blue arrows illustrate pressure buildup. (b) Pressure buildup gave rise to the formation of a stacking fault due to the slip. Further slip accompanied by redistribution of surface atoms removes the stacking fault (not shown). (c) A new stacking fault appears resulting in the further extrusion of the metal. (d) Pressure inside a Pt particle as a function of time at zero temperature and 600 °C. (e) A cross section of the particle showing the surface atoms (blue) and atoms in non-fcc configurations corresponding to point (1) in (d). An intrinsic stacking fault is observable. Stacking faults and twin boundaries corresponding to points (2) and (3) in plot (d) when a part of the material is extruded are also shown.

defect. This resulted in a partial extrusion of the metal from the onion [Fig. 4(b)]. Because of further pressure buildup, sliding occurred along another (111) glide plane, as schematically depicted in Fig. 4(c). At finite temperatures pressure and, thus, the resolved shear stresses on slip planes were always lower than  $\sigma_T$ .

A planar defect can vanish after the glide of a trailing partial, leaving eventually the perfect lattice. As the contraction in our simulations (about 1 cm/sec) is 7 orders of magnitude faster than in the experiments, we did not see the disappearance of stacking faults in the simulations with the setup described above. To account for a slower contraction rate, we also carried out simulations with a different setup: After the appearance of an ISF, the external potential was fixed (pressure was not removed), and the evolution of the system at 600 °C was simulated by molecular dynamics at the time scale up to 200 nsec. We found that the ISF can indeed disappear due to a fast motion of a trailing partial dislocation.

In our simulations we saw predominantly the formation of ISFs, but twins also appeared. For example, a twin boundary (single plane of atoms in the hcp configuration) can be seen in the lower part of Fig. 4(e). In Au and Pt crystals with diameters of several nanometers, twins are known [24] to appear and disappear at the temperatures of the experiment due to dislocation motion on the submicrosecond time scale. This time scale is consistent with our simulations and is many orders of magnitude below the time resolution of our experiments which is given by the minimum exposure time of an image (0.1 s). Defects appearing, migrating, and vanishing on a shorter time scale are not accessible to the observation. Hence we can conclude that the nucleation and glide of short-living dislocations is consistent with our observation of defect-free metal crystals during the deformation, as has already been suggested in an early study [25].

A considerable influence of electron irradiation on the deformation behavior of the metals is not expected because the threshold electron energy for the displacement of bulk atoms in Au, Pt, or Mo is higher than 1000 keV [26]. A smaller contribution of radiation-enhanced diffusion, on the other hand, cannot be excluded.

In conclusion, the slow deformation of nanometer-sized Au or Pt crystals is governed in a wide temperature range by the activity of short-lived dislocations. Nucleation, glide, and vanishing of the dislocations happens on a submicrosecond time scale. Since the single events of this mechanism happen on such a short time scale, it might be impossible to prove the existence of these dislocations directly with the presently available experimental techniques. All other defects that are accessible to electron microscopy observation can be excluded above a certain temperature. Creep by volume or surface diffusion can also be excluded. We also showed that the vacancy formation energy is larger in small particles than in the bulk, resulting in a substantial drop in vacancy concentration and thus

lowering the diffusion-mediated mass transfer. This is of high importance for the applicability of nanocrystalline materials and shows that they may be more stable against creep under load at high temperature than materials with larger grain size.

The authors thank A. Kuronen, T. Järvi, and K. Albe for discussions. This work was supported by DFG (Ba1884/4-2), a DAAD and ETC exchange grant (No. D/05/51651), and the Academy of Finland under CONADEP and OPNA projects and the Centre of Excellence program. We are also indebted to the Finnish IT Center for Science for generous grants of computer time.

---

\*banhart@ipcms.u-strasbg.fr

- [1] H. Gleiter, *Acta Mater.* **48**, 1 (2000).
- [2] S. Yip, *Nature (London)* **391**, 532 (1998).
- [3] E. Arzt, *Acta Mater.* **46**, 5611 (1998).
- [4] J. Schiøtz *et al.*, *Nature (London)* **391**, 561 (1998).
- [5] K. W. Jacobsen *et al.*, *Nature Mater.* **1**, 15 (2002).
- [6] V. Yamakov *et al.*, *Nature Mater.* **1**, 45 (2002).
- [7] H. van Swygenhoven and J. A. Weertman, *Mater. Today* **9**, 24 (2006).
- [8] E. Rabkin and D. J. Srolovitz, *Nano Lett.* **7**, 101 (2007).
- [9] J. I. Pascual *et al.*, *Science* **267**, 1793 (1995).
- [10] Z. W. Shan *et al.*, *Science* **305**, 654 (2004).
- [11] Y. Choi *et al.*, *J. Appl. Phys.* **94**, 6050 (2003).
- [12] L. Sun *et al.*, *Science* **312**, 1199 (2006).
- [13] P. W. Sutter and E. A. Sutter, *Nature Mater.* **6**, 363 (2007).
- [14] J. X. Li and F. Banhart, *Adv. Mater.* **17**, 1539 (2005).
- [15] F. Banhart, *Rep. Prog. Phys.* **62**, 1181 (1999).
- [16] A. V. Krasheninnikov and F. Banhart, *Nature Mater.* **6**, 723 (2007).
- [17] D. Ugarte, *Chem. Phys. Lett.* **209**, 99 (1993).
- [18] See EPAPS Document No. E-PRLTAO-101-006842 for supplementary text and figures. For more information on EPAPS, see <http://www.aip.org/pubservs/epaps.html>.
- [19] L. Sun *et al.*, *Appl. Phys. Lett.* **89**, 263104 (2006).
- [20] H. W. Qi and M. P. Wang, *Physica (Amsterdam)* **334B**, 432 (2003).
- [21] M. Müller and K. Albe, *Acta Mater.* **55**, 3237 (2007).
- [22] G. Bertoni *et al.*, *Phys. Rev. B* **71**, 075402 (2005).
- [23] At zero temperature, an ISF was formed instantly by the sliding of a part of the crystal along (111) planes. The crossover between homogeneous slip and dislocation-mediated mechanisms depended not only on temperature but also on the actual shearing stress, which can be estimated as  $\sigma \sim P(a/R)^2 \cos(\alpha)$ , where  $P$  is the internal pressure,  $R$  and  $a$  are the radii of the particle and the orifice, respectively, and  $\alpha$  is the angle between the symmetry axis and the slip plane. Depending on temperature and  $\alpha$ ,  $\sigma$  can be both under or above the theoretical shear stress which resulted in a different behavior.
- [24] T. T. Järvi *et al.*, *Phys. Rev. B* **75**, 115422 (2007).
- [25] J. C. Li, *Trans. Soc. Pet. Eng.* **227**, 239 (1963).
- [26] P. Jung, in *Atomic Defects in Metals*, edited by H. Ullmaier, Landolt-Börnstein, New Series, Group III, Vol. 25 (Springer, Berlin, 1991), pp. 1–87.